Metallurgical and Materials Transactions 46A (2013)
286-293

Medium–Alloy Manganese–Rich Transformation–Induced Plasticity Steels

D. W. Suh[a], J. H. Ryu[a], M. S. Joo[a], H. S. Yang[b], K. Y. Lee[b], H. K. D. H. Bhadeshia[a,c]

[a] *Graduate Institute of Ferrous Technology, POSTECH, Republic of Korea*

[b] *Technical Research Laboratories, POSCO, Republic of Korea*

[c] *Materials Science and Metallurgy, University of Cambridge, U.K.*

Abstract

The manganese concentration of steels which rely on transformation–induced plasticity is generally less than 2 wt%. Recent work has highlighted the potential for strong and ductile alloys containing some 6 wt% of manganese, but with aluminium additions in order to permit heat treatments which are amenable to rapid production. However, large concentrations of aluminium also cause difficulties during continuous casting. Alloy design calculations have been carried out in an effort to balance these conflicting requirements, whilst maintaining the amount of retained austenite and transformation kinetics. The results indicate that it is possible by adjusting the carbon and manganese concentrations to reduce the aluminium concentration, without compromising the mechanical properties or transformation kinetics. The deformation–induced transformation of retained austenite is explained quantitatively, for a range of alloys, in terms of a driving force which takes into account the very fine state of the retained austenite.

Email addresses: dongwoo1@postech.ac.kr (D. W. Suh), hkdb@cam.ac.uk (H. K. D. H. Bhadeshia)

Keywords: transformation-induced plasticity, steel, manganese, austenite, stability

1. Introduction

Work by Miller [1] established the possibility of alloys containing a medium manganese concentration, Fe–0.11C–5.7 Mn wt%, in order to generate a mixed microstructure of ferrite and austenite by intercritical annealing. The plasticity obtained during the deformation–induced martensitic transformation of austenite (TRIP) led to impressive values of total elongation (34–19%) for tensile strengths in the range 875–1200 MPa. The time periods for intercritical annealing were in the range 1–16 h.

In an effort to make the process more amenable to industrial production, Suh and co–workers [2] added up to 3 wt% of aluminium to the steel, on the basis that this solute increases the free energy change associated with the austenite to ferrite transformation [3]. This has the effect of increasing the temperature at which the steel can be intercritically annealed, thus permitting the time period of annealing to be reduced to just two minutes [2]. However, it is considered that 3 wt% is too large a concentration from the point of view of steel manufacture by continuous casting because of the possibility of nozzle clogging [4]. The purpose of the present work was to see if a similar alloy system can be designed with a reduced aluminium concentration of 2 wt%, a content which is considered acceptable from a steelmaking point of view. It may be possible to compensate for the reduction in aluminium concentration by altering the carbon and manganese concentrations, and this formed the motivation for the present work.

2. Experimental method

Table 1 lists the chemical compositions of the alloys. Compared to the previous work based on Fe–0.12C–5.8Mn–0.47Si–3.1Al wt% [2], the alu-

minium content is reduced to 2 wt%. The carbon and manganese concentrations were adjusted systematically using phase diagram calculations in order to obtain a comparable austenite fractions during intercritical annealing. Fig. 1 shows the change of equilibrium fraction of austenite estimated using the Thermo-Calc software [5] with TCFE 6 database [6]. It clearly is possible in principle to maintain the austenite content in the temperature range of intercritical annealing.

Table 1: Chemical compositions (wt%) of alloys

Sample	C	Mn	Si	Al
Alloy 1	0.11	4.5	0.45	2.2
Alloy 2	0.075	5.1	0.49	2.1
Alloy 3	0.055	5.6	0.49	2.2

Ingots $300 \times 150 \times 100$ mm were prepared by vacuum–induction melting, after which they were reheated to 1473 K (1200 °C) for 2 h and hot–rolled to 3 mm thick sheet, with a finish–rolling temperature above 1000 K (727 °C), before the samples were finally air–cooled. After pickling in a 10 % HCl solution, the sheets were cold–rolled to 1 mm in thickness.

The samples were then annealed using an infrared heating furnace at temperatures in the range 973 to 1053 K (700 to 780 °C) in 20 K (°C) steps, with a holding time during annealing of 120 s before cooling to ambient temperature. The heating and cooling rates to and from the annealing temperature were in all cases ± 10 Ks^{-1} ($^{\circ}\mathrm{C\,s}^{-1}$).

The microstructures were characterised using light and scanning electron microscopy (SEM), and electron back–scattered diffraction (EBSD). The fraction of austenite was determined using X–ray diffraction with Cu K_α radiation; for this purpose the specimens were prepared by mechanical polishing followed by chemical polishing in a 10 % $HF+H_2O_2$ solution in

order to remove any deformed surface which would influence the retained austenite. The integrated intensities of $(200)\alpha$, $(211)\alpha$, and $(220)\gamma$, $(311)\gamma$ reflections were used to quantitatively determine the austenite content [7]. Tensile tests were conducted on a universal testing machine at a crosshead speed of $2\,\mathrm{mm\,min^{-1}}$, using sub–sized test coupons according to the ASTM [8].

3. Results and discussion

3.1. Microstructures

Fig. 2 shows the microstructures of the hot–rolled steels. The dark grey matrix is martensitic, while the grey streaks represent δ–ferrite retained due to non–equilibrium cooling during solidification, and spread out into layers during hot–rolling [9]. Optical microscopy was conducted for all annealing treatments and the results are available for inspection, but the phase maps in Fig. 3 have much greater clarity. They reveal relatively coarse regions of recrystallised–ferrite and much finer ferrite grains which still contain sub–grain boundaries. The black lines in Fig. 3 correspond to large angle grain boundaries of which misorientation is larger than 15°, whereas the blue lines are low–misorientation sub–grain boundaries.

The grains with green colour are extremely fine austenite grains, located within the relatively fine–grained ferrite regions. The quantitative measurements presented in Fig. 4 confirm a size of the order of $0.3\,\mu\mathrm{m}$, insensitive to the annealing conditions, or even alloy composition within the range studied. The austenite grains are equiaxed and are mostly isolated rather than in the form of allotriomorphs, indicating that they nucleate at triple points within the fine–grained ferrite, and have a limited growth rate.

The presence of the coarse ferrite grains indicates that they were the first to recrystallise during annealing, and that their growth is stifled subsequently by the formation of austenite in the unrecrystallised regions. This explains why the coarse ferrite grains are essentially free from austenite.

The boundary character in the phase maps suggests that the coarse ferrite grains are completely recrystallised but the small angle boundaries observed in the fine–grained regions indicates incomplete recrystallisation. The observed microstructure is comparable to that from previous work [2], but more homogeneous because the lower aluminium concentration leads to a reduced content of the coarse ferrite which originates from the δ–ferrite formed during solidification.

The fraction of austenite is plotted in Fig. 5 for the complete set of experiments conducted, along with that expected from equilibrium (calculated using Thermo–Calc). Given that the alloys were designed to show similar austenitisation behaviour (Fig. 1), the experimentally determined austenite content does not differ much between the different alloys – it increases gradually up to 1033 K (760 °C) but then drops sharply for samples annealed at 1053 K (780 °C). This is because when the volume fraction of austenite becomes large, a quantity decomposes by martensitic transformation on cooling to ambient temperature as is evident from the dilatometric curves presented in Fig. 6. The reasons for the reduced stability of the austenite when the volume fraction is large include the dilution of solute content (carbon, manganese) and secondly, it is well known that the stability of the austenite decreases with increasing grain size [10, 11]. Fig. 7 is a representative transmission electron micrograph in which the austenite grains subjected to energy dispersive X-ray microanalysis are marked. The data thus obtained are summarised in Table 2 and the measured values compare within experimental error with those expected from equilibrium. Although there may not be an exact match with equilibrium, it is obvious that Mn is likely to be partitioned into austenite. It is noted that cementite was not observed in the annealed samples since the annealing temperatures used exceed the the dissolution temperature of that carbide.

Table 2: Mn content in austenite after annealing at 720 °C (in wt%). The calculated equilibrium concentrations are also stated for comparison.

	Measured Mn	Equilibrium Mn	No. of grains measured
alloy 1	7.4 ± 1.2	8.8	22
alloy 2	8.1 ± 0.9	9.6	26
alloy 3	9.1 ± 0.8	10.3	32

3.2. Mechanical behaviour and austenite stability

Fig. 8 (a) to (c) show representative stress–strain curves. The mechanical properties are summarised in Fig. 9. The yield strength decreases with an increase in the annealing temperature, possibly because of the corresponding greater degree of softening of the initially cold–deformed ferrite. The tensile strength on the other hand, increases with the annealing temperature and a close examination of Fig. 8 shows that this is entirely due to the fact that the work hardening rates are greatest for samples annealed at the highest of temperatures, i.e., containing the largest amount of retained austenite.

The observed variations in elongation Fig. 9 are particularly interesting, and are attributed to changes in the stability of the retained austenite. For annealing temperature ranging from 973–1033 K (700–760 °C), a maximum elongation is obtained for the annealing temperature of 993 K (720 °C) in Alloy 1 but that in Alloy 3 decreases monotonously; Alloy 2 shows a weak maximum at 993 K (720 °C). Since the deformation–induced martensite plays a role in inducing more homogeneous deformation (avoiding plastic instabilities) [12, 13], there is an optimum austenite stability which is conducive to the late onset of necking during tensile tests. The austenite should not all decompose at an early stage of deformation, and it should not be so stable that assistance from transformation plasticity in preventing necking is absent [14].

The symbols in Fig. 10 are experimental data which show how the retained austenite decomposes as a function of plastic strain. The austenite is particularly stable in Alloy 1 annealed at 973 K (700 °C) and the deformation–induced transformation becomes more rapid as the annealing temperature is increased. It is therefore expected that the optimum stability of austenite consistent with homogeneous deformation will be obtained at an intermediate annealing temperature. Compared with Alloy 1, the austenite in Alloy 3 annealed at 973 K (700 °C) is less stable and thus an increase of annealing temperature by 20 K (°C) reduces the mechanical stability of austenite to such an extent that the homogeneous deformation is exhausted at an early stage in the tensile test.

As pointed out, there are two major parameters controlling the stability of austenite, the concentrations of alloying elements and the grain size. According to the Sherif et al. [15], the influence of the alloy composition can be expressed as follows,

$$\frac{V_\gamma}{V_\gamma^\circ} = \exp\left(-k_1 \Delta G^{\gamma\alpha'} \epsilon\right). \tag{1}$$

Here, V_γ° is the austenite fraction prior to deformation, and V_γ the corresponding fraction at any value of the true plastic strain ϵ. The parameter k_1 is a fitting constant. This equation does not include any effect due to the size of the austenite regions, so only the chemical driving force $\Delta G^{\gamma\alpha'} = G^{\alpha'} - G^{\gamma}$ (J mol^{-1}), a function of the chemical composition of the austenite, was considered. In the present study, the term was modified to reduce the magnitude of $\Delta G^{\gamma\alpha'}$ by ΔG_S, where the latter depends on the austenite grain size. ΔG_S was calculated from the reduction in the martensite–start temperature, ΔM_S, caused purely by the size of the transforming region, according to Ref. [11] as follows:

$$\Delta M_s = \frac{1}{b} \ln\left[\frac{1}{aV_\gamma}\left\{\exp\left(-\frac{\ln(1-f)}{m}\right) - 1\right\} + 1\right] \tag{2}$$

Here, V_γ is average volume of an austenite grain, f is the first detectable martensite fraction (0.01) and m is the aspect ratio of martensite plate (0.05), respectively. a and b are constants of 1.57×10^{-21} μm and 0.253 respectively [11]. The influence of austenite grain size on the reduction of the martensite–start temperature, ΔM_S, was converted into the extra free energy required for the transformation due to the size effect, ΔG_S. The free energies were all calculated using ThermoCalc and the TCFE 6 database assuming an equilibrium concentration of substitutional solutes, but the carbon content was estimated from a mass balance between the ferrite and measured austenite fraction. The assumption on the substitutional solutes is reasonable given the large degree of partitioning of manganese in Table 2 when compared with the average values listed in Table 1. The lines in Fig. 10 shows the calculated austenite fractions during deformation. The stability of the austenite in all cases is reasonably captured using a single fitting parameter, $k_1 = 0.008$ mol J^{-1}. Comparing Figs. 10 (a) and (b) suggests that the austenite has worse stability as carbon is replaced by manganese during alloy design. On the basis of equation 1, this effect has its origin in the larger influence of carbon on the driving force for martensitic transformation.

From the kinetics of deformation–induced transformation, the contribution of martensite formation on the work–hardening behaviour was estimated. Fig. 11 shows the calculated hardness increment accompanying to the martensite formation during straining in Alloy 1, with the hardness of martensite evaluated following Ion et al. [16] and the hardness ratio of austenite to martensite is assumed to be 0.6 [17]. The increments of hardness corresponding to the strain consistent with the ultimate tensile strength, are $\Delta H_V^{700} = 6.9$, $\Delta H_V^{720} = 46.7$, $\Delta H_V^{740} = 58.4$ and $\Delta H_V^{760} = 65.6$. These can be used to estimate strength increments due to work–hardening caused by martensitic transformation [18], as $\Delta\sigma^{700} = 16$ MPa, $\Delta\sigma^{720} = 84$ MPa,

$\Delta\sigma^{740} = 118$ MPa and $\Delta\sigma^{760} = 150$ MPa.[1] Comparison with the observed work–hardening, $\Delta\sigma^{700} = 42$ MPa, $\Delta\sigma^{720} = 107$ MPa, $\Delta\sigma^{740} = 246$ MPa and $\Delta\sigma^{760} = 369$ MPa, indicates that the real hardening is much larger than that expected from the hardness increment due to martensite formation, except for the case of annealing at 993 K (720 °C). The discrepancy may arise from known effects associated with the creation of dislocation debris during transformation, and the composite effect of multiphase deformation [13, 19].

4. Conclusions

Alloys relying on transformation–induced plasticity, containing a relatively large manganese concentration and a reduced aluminium concentration have been designed and validated experimentally. It is found that:

1. Reducing either the carbon or manganese concentrations can permit the aluminium content to be reduced without compromising the required 15 – 25 % retained austenite generated during intercritical annealing for short time periods.
2. The structure obtained is found to contain incredibly fine and equiaxed grains of retained austenite, and the approximately 0.3μm scale of these grains is insensitive to the annealing temperature over the range studied. Furthermore, the fine scale adds significantly to the stability of the retained austenite. The formulation combining the influence of chemical driving force and grain size captures reasonably the mechanical stability of austenite and the kinetics of deformation–induced transformation in the investigated alloys.
3. For the range of alloys studied, it is noteworthy that the dependence of tensile properties of the composition itself is not large with respect to variations in the carbon and manganese levels. This bodes well for

[1] Following [18], $\Delta\sigma$ (kg/mm^2)$=\frac{\Delta H}{3}(0.1)^n$, n is strain hardening coefficient

mass manufacture where strict composition specifications are hard to maintain, and where solidification–induced segregation can produce a heterogeneous distribution of the the intended concentration.

Acknowledgments: The authors are grateful for support from the POSCO Steel Innovation Programme, and to the World Class University Programme of the National Research Foundation of Korea, Ministry of Education, Science and Technology, project number R32–2008–000–10147–0.

[1] R. L. Miller: Metallurgical Transactions 3 (1972) 90–912.

[2] D. W. Suh, S. J. Park, T. H. Lee, C. S. Oh, S. J. Kim: Metallurgical and Materials Transactions A 41A (2010) 397–408.

[3] H. Aaronson, P. G. Domian, H.A.: TMS-AIME 236 (1966) 781–796.

[4] S. Abdelaziz, G. Megahed, I. El-Mahallawi, H. Ahmed: Ironmaking and Steelmaking 36 (2009) 432–441.

[5] B. Sundman, B. Jansson, J. Andersson: CALPHAD 9 (1985) 153–190.

[6] Bratberg: TCFE6-TCS Steels / Fe-Alloys Database, Version 6.2: Tech. rep.: Thermo-Calc software AB: Stockholm, Sweden (2011).

[7] C. F. Jatczak: SAE Technical Paper Series 800426: Tech. rep.: SAE (1980).

[8] ASTM E8M3 Standard Test Method for Tension Testing of Metallic Materials.

[9] H. Yi, Lee.K.Y., H. Bhadeshia: Materials Science and Technology 27 (2011) 525–529.

[10] P. Brofman, G. Ansell: Metallurgical Transactions A 14A (1983) 1929–1931.

[11] H. S. Yang, H. K. D. H. Bhadeshia: Scripta Materialia 60 (2009) 493–495.

[12] W. Gerberich, G. Thomas, E. Parker, V. Zackay: Metastable austenite: Decomposition and strength: in: Second International Conference on Strength of Metals and Alloys: ASM International, Ohio, USA, 1970: pp. 984–899.

[13] H. K. D. H. Bhadeshia: ISIJ International 42 (2002) 1059–1060.

[14] J. M. Jang, S. J. Kim, N. H. Kang, K. M. Cho, D. W. Suh: Metals and Materials International 15 (2009) 909–916.

[15] M. Sherif, M. Garcia Mateo, T. Sourmail, H. Bhadeshia: Materials Science and Technology 20 (2004) 319–322.

[16] J. Ion, L. Anisdahl: Journal of Materials Science and Technology 65 (1997) 261–267.

[17] Q. Furnemont, M. Kempf, P. Jacques, M. Goken, F. Delannay: Materials Science and Engineering A328 26–32.

[18] J. Cahoon, W. Broughton, A. Kutzak: Metallurgical Transactions 2 (1971) 1979–1983.

[19] Y. Tomota, K. Kuroki, T. Mori, I. Tamura: Materials Science and Engineering 24 (1976) 85–94.

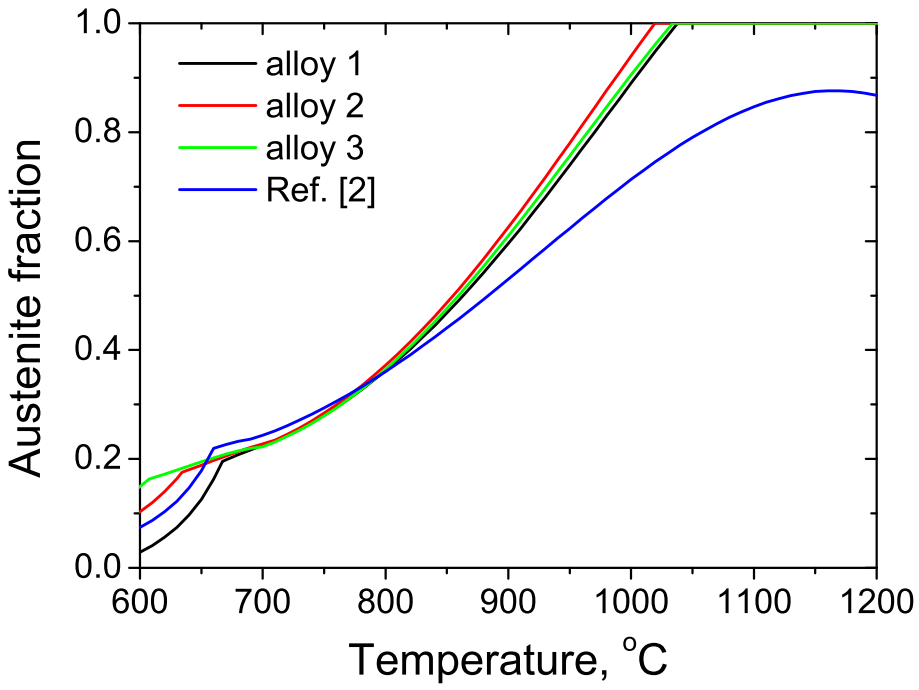

Figure 1: Equilibrium phase fraction of investigated alloy at elevated temperature

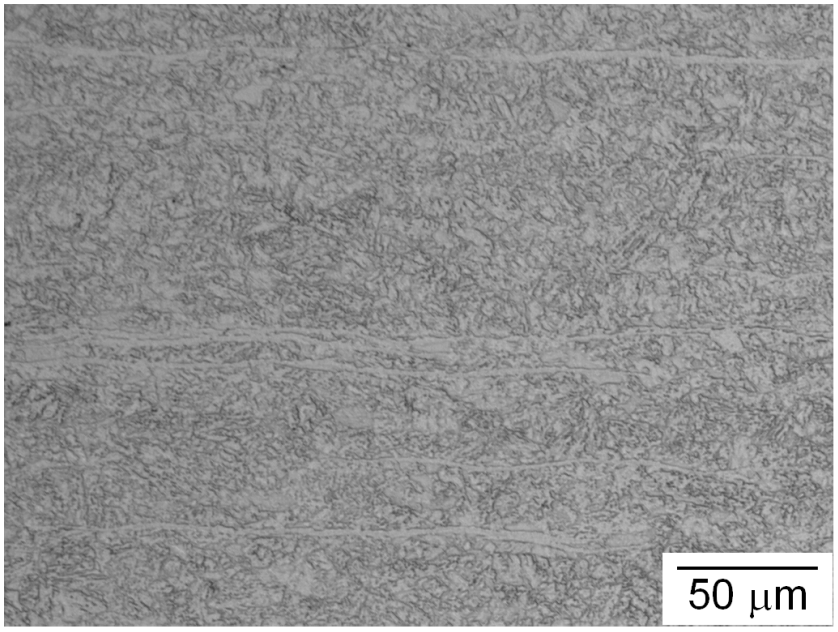

(a)

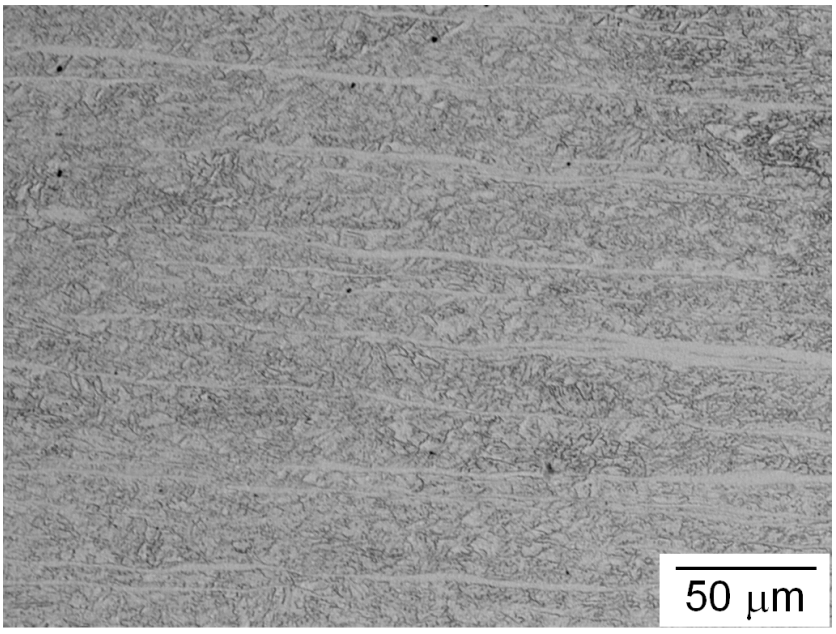

(b)

Figure 2: Optical micrographs of hot-rolled (a) Alloy 1, (b) Alloy 2. (continued on next page)

(c) 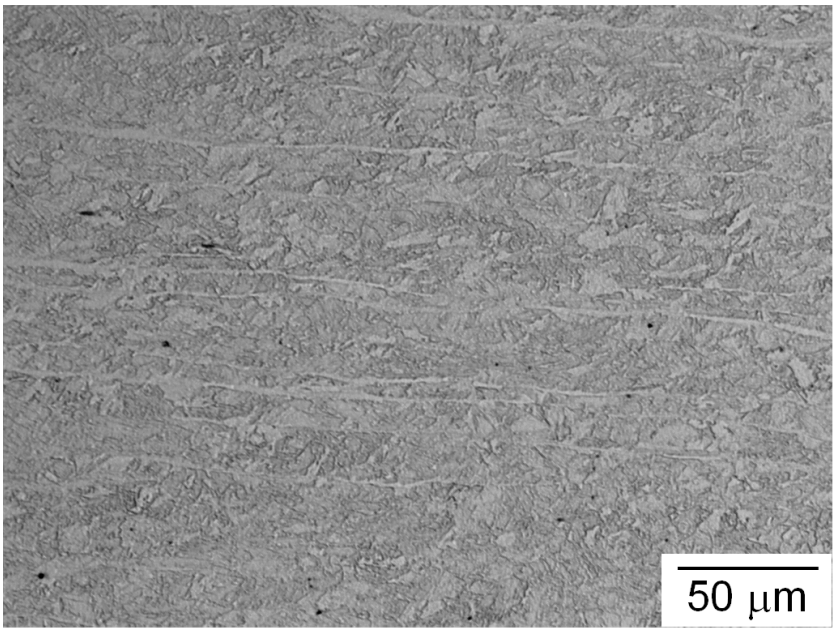

Figure 2: (continued from previous page) (c) Optical micrographs of hot-rolled Alloy 3

(a)

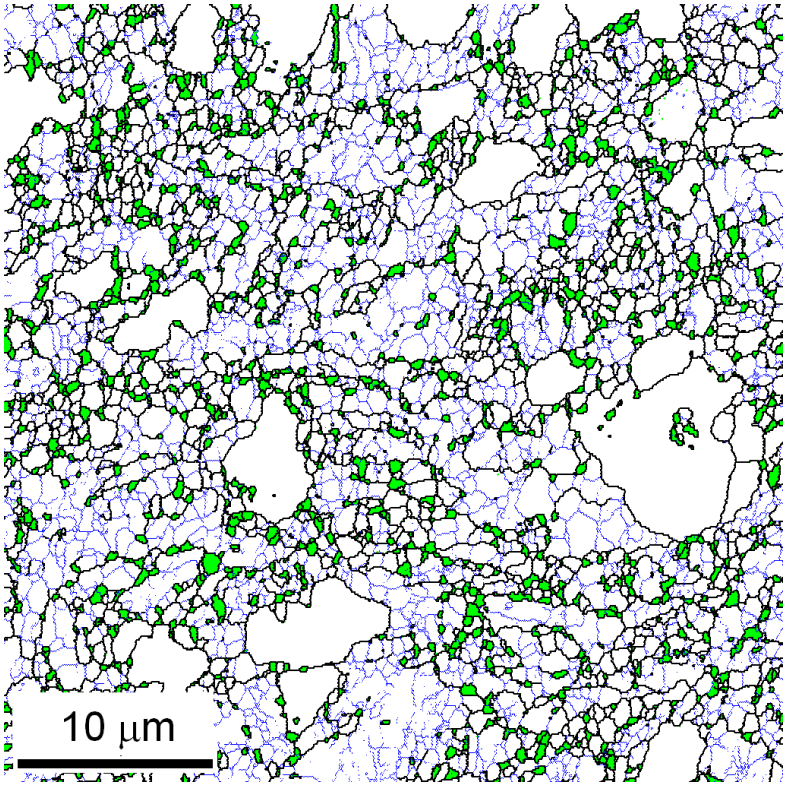

(b)

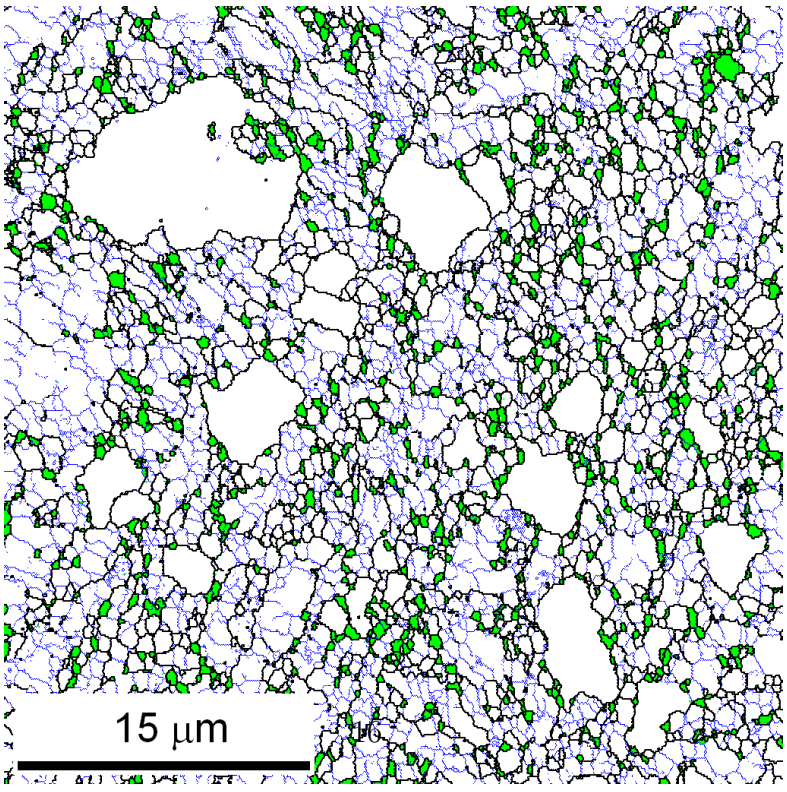

Figure 3: Phase maps of annealed (a) Alloy 1, (b) Alloy 2, following annealing at 993 K (720 °C). (continued on next page).

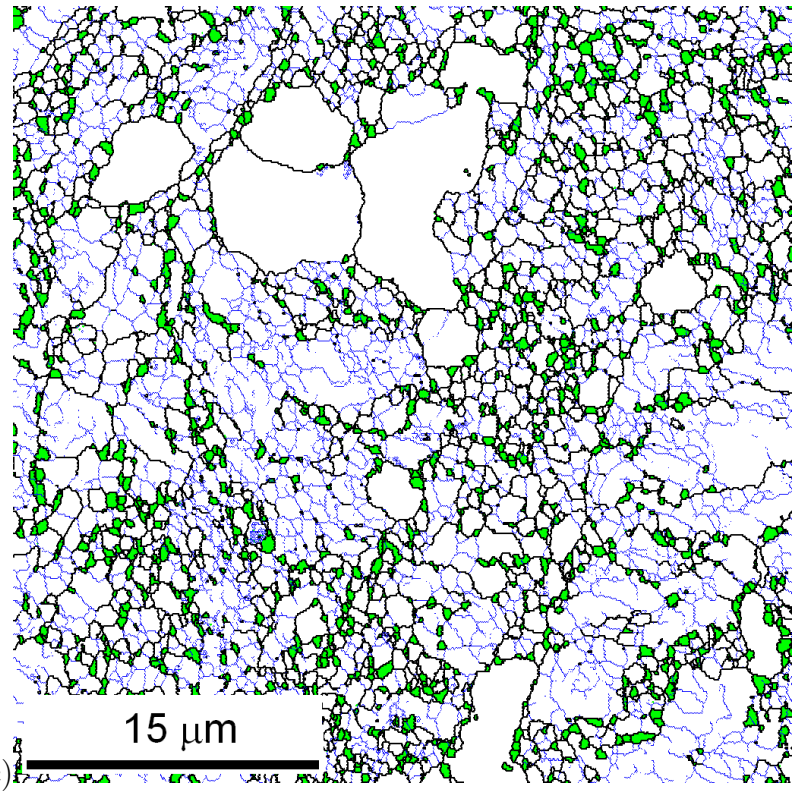

(c)

Figure 3: (continued from previous page) (c) Phase map of annealed Alloy 3 following annealing at 993 K (720 °C).

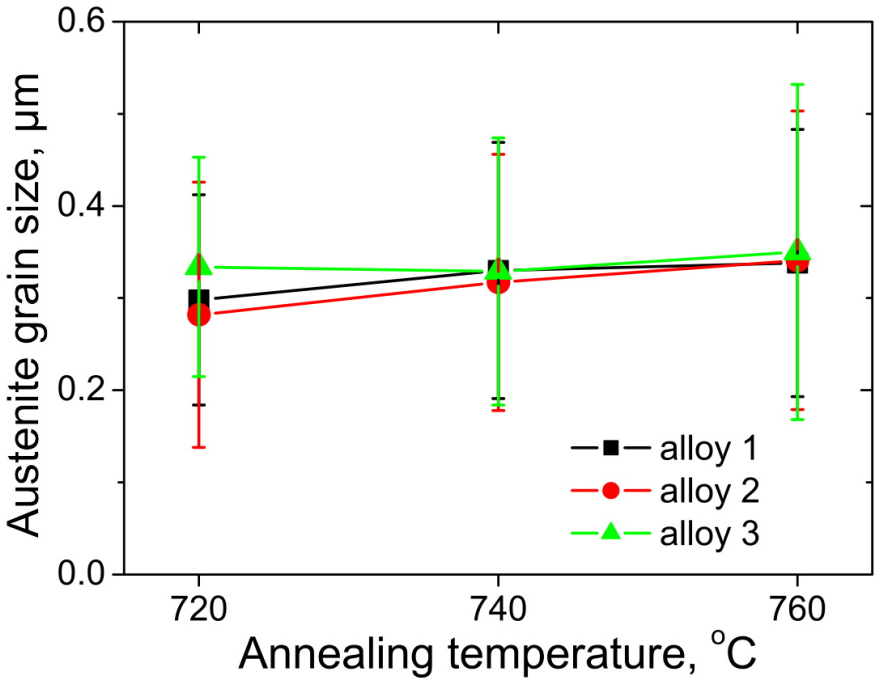

Figure 4: Austenite grain size as a function of annealing temperature.

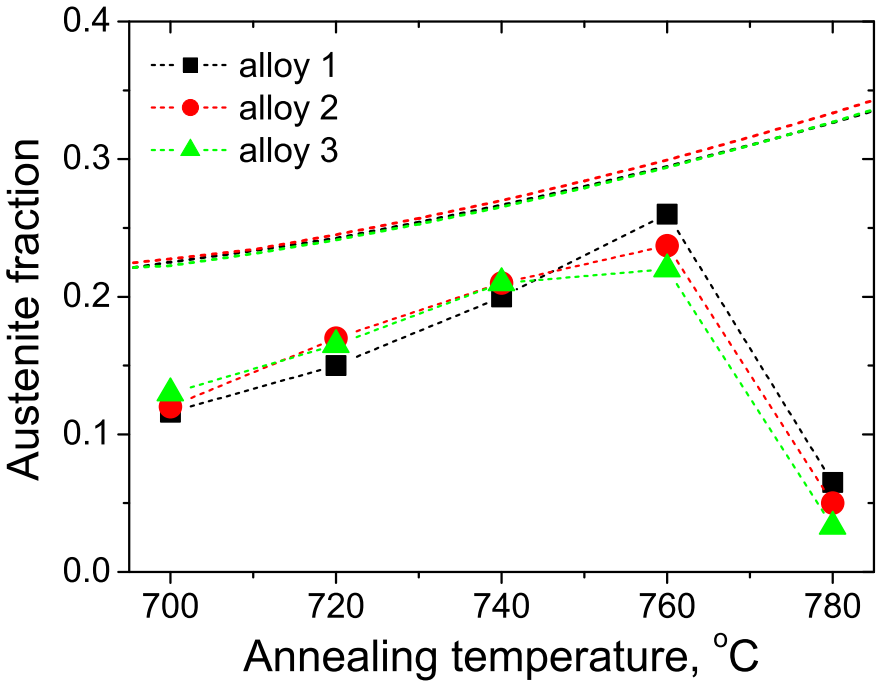

Figure 5: Austenite fraction as a function of annealing temperature. The lines without points represent the calculated equilibrium fractions.

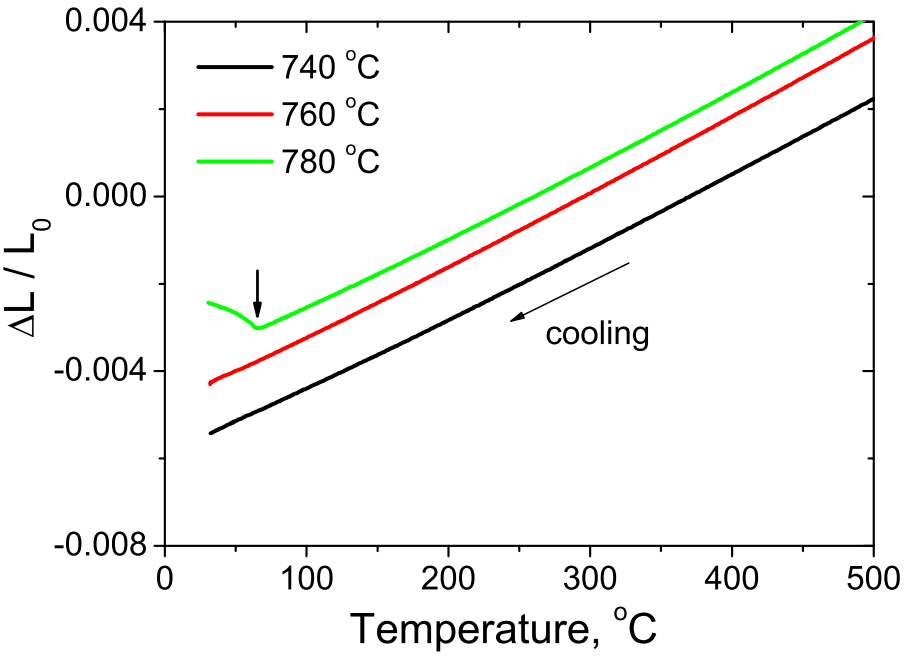

Figure 6: Dilatation curves of Alloy 1 on subsequent cooling after annealing at each temperature. Arrow indicates the start of martensite transformation.

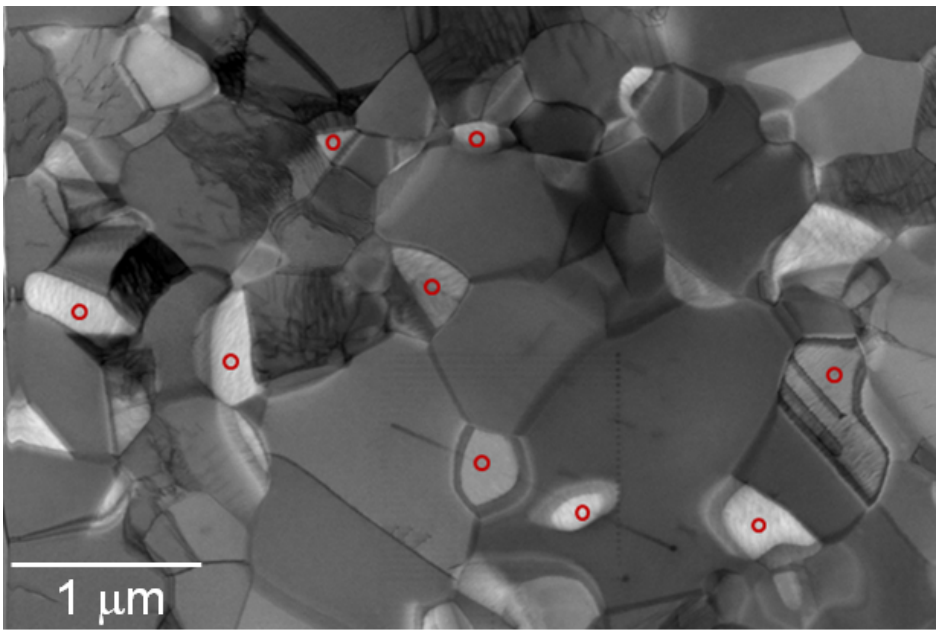

Figure 7: TEM micrograph of alloy 3 annealed at 720 ° C

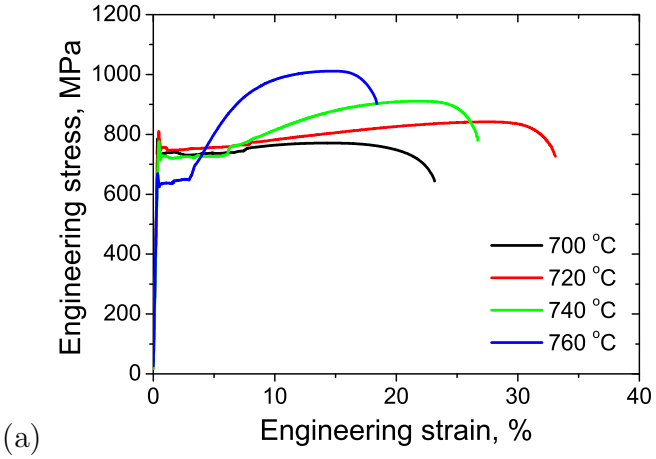

(a)

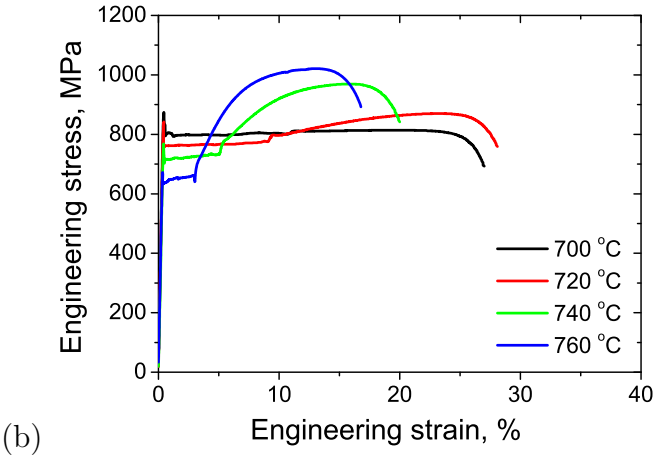

(b)

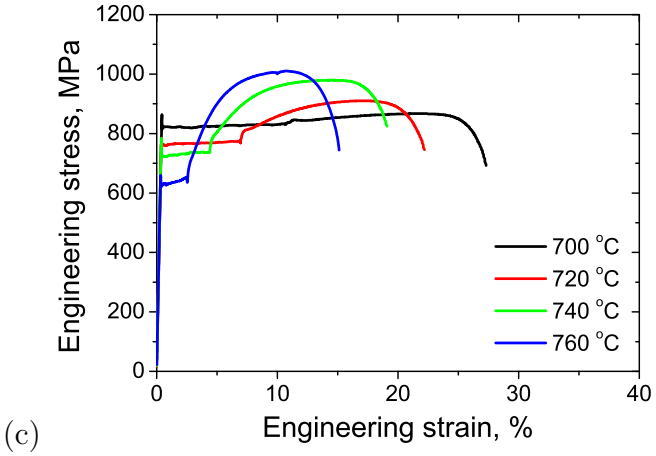

(c)

Figure 8: Stress–strain curves of annealed (a) Alloy 1, (b) Alloy 2 and (c) Alloy 3

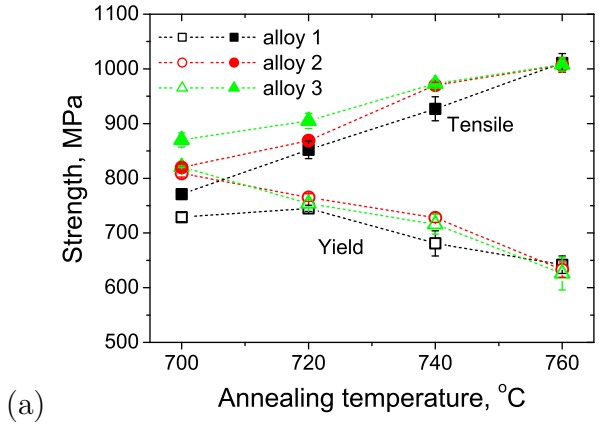

(a)

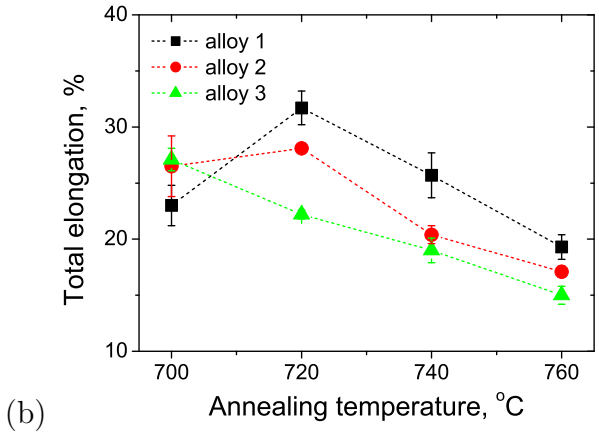

(b)

Figure 9: (a) Tensile and yield strength, (b) total elongation of annealed alloys

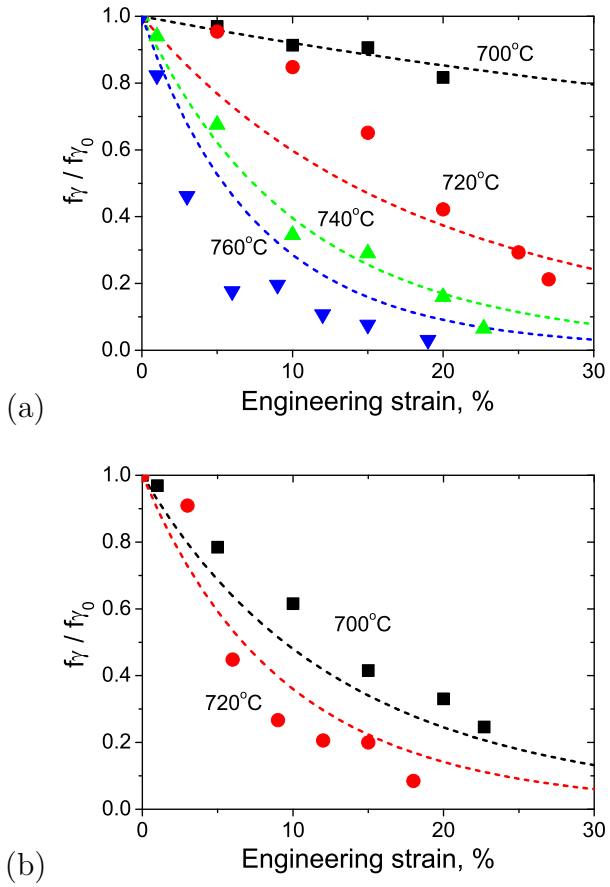

Figure 10: Austenite fractions in (a) Alloy 1 and (b) Alloy 3 as a function of strain. Symbols are measured values and lines are calculated ones.

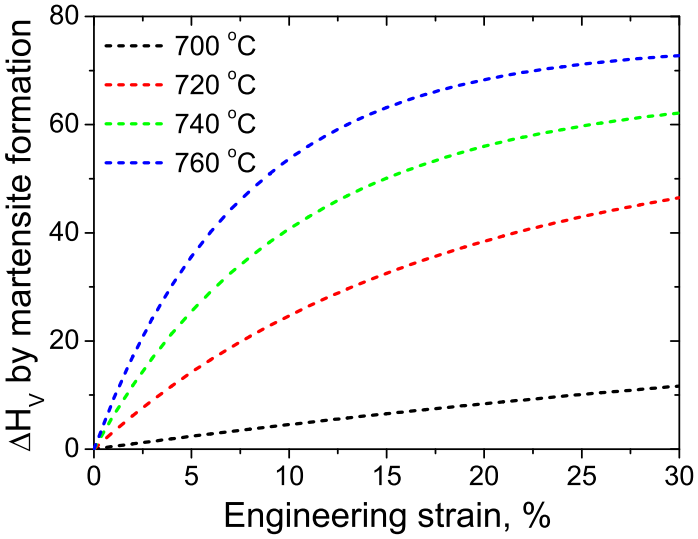

Figure 11: Calculated hardness increment from the strain–induced martensite transformation in Alloy 1.